Hindawi
Advances in Civil Engineering
Volume 2023, Article ID 3378168, 15 pages
https://doi.org/10.1155/2023/3378168

Research Article

Effect of Reinforcement Forms on the Load Bearing Capacity of Prefabricated Box Culvert

Pengfei Xu,[1] Li Wang,[1] Jian Chen,[2] Ming Li,[3,4] Rui Guo,[1] Yajun Xie,[5] and Da Zong[3]

[1]*Huai'an Water Conservancy Survey and Design Institute Co., Ltd, No. 9, Shenzhen Rd., Huai'an 223005, China*
[2]*Jianhua Building Materials Technology (Huai'an) Co. Ltd, No. 1, Yanbei Avenue East Rd., Huai'an 223215, China*
[3]*College of Civil and Transportation Engineering, Hohai University, No. 1 Xikang Road, Nanjing 210024, China*
[4]*School of Geography and Planning, Huaiyin Normal University, 111 West Changjiang Road, Huaian 223300, China*
[5]*Huai'an Water Conservancy Bureau, No. 9 Shenzhen Road, Huai'an 223005, China*

Correspondence should be addressed to Da Zong; zongd@hhu.edu.cn

Received 12 April 2023; Revised 22 October 2023; Accepted 14 November 2023; Published 8 December 2023

Academic Editor: Zhipeng Zhao

Box culvert structure was an essential part of modern infrastructure. Due to the advantages of low pollution and convenient construction, the prefabricated box culvert (PBC) has been gradually utilized in engineering. However, the investigations on load bearing capacity of PBC in different reinforcement forms with same reinforcement ratios were still lack. In the present research, one PBC specimen was tested and discussed by the finite-element analysis (FEA) on load bearing capacity under four-point bending. The load bearing capacity of another three PBCs in different reinforcement forms with the same reinforcement ratios was discussed by the FEA. Results of experimental and numerical investigations showed that: (1) a number of flexural cracks were observed in the midspan bottom of upper slab of PBC, and finally shear failure was observed in bending–shear zone of upper slab of PBC; (2) the number of concrete cracking, plastic deformation of PBC, and stress of rebars reduced by increasing the area of tensile rebars in PBC with reducing the area of compressive rebars under same reinforcement ratios; (3) the ductility and load bearing capacity of PBC increased by increasing the area of tensile rebars with reducing the area of compressive rebars.

1. Introduction

Box culvert (BC) structure, which is used in bridging over streams, drainages, sewage pipelines, highway bridges, and other projects, is an essential part of modern infrastructure [1–4]. The investigations on the application of BC have extensively conducted in scholars, which significant advances in design, construction, and materials of BC [5]. Scholars have mainly researched on the interaction of truck wheel load and circumambient backfill pressure with BC. The properties of the soil surrounding the BC, such as its composition, density, and strength, significantly impacted the stability and performance of the structure. Based on the measured data of displacement and strain of 10 concrete box culverts in each construction stage under shallow overburden soil, an experimental study on the moving load effect at different overburden soil heights above the culvert was carried out [6]. The results showed that the influence of moving load on the BC decreases with the increase of overburden soil thickness. Wood et al. [7] observe the mechanical properties of the tested culverts by increasing thickness of the overburden on top of culverts and applying vehicle live load. As the working conditions of BC components became more and more severe, reducing the external load of BC has been paid more attention by the scholars. The effects of boundary conditions [8, 9], vertical soil pressure [10], soil stiffness [11], vehicle load [12], construction error [13], fatigue behavior [14], shear behavior [15], blast loads [16], and geometric construction [17] on the performance of BC were analyzed efficiently by finite-element analysis (FEA). Philip et al. [18] conduct model tests and FEA to examine the properties of top-filling materials affected the bending moment characteristics of BC under bridge design. The study revealed that the use of top-filling material (geofoam) significantly decreases the bending moment at various sections of the BC. This approach also offers an eco-friendly solution to decrease lateral earth

pressure exerted on the outer wall of BC. Moreover, the centrifuge model tests simulate slope failure, change retaining wall bearing pressure, and change soil–structure interactions to reproduce the actual ground stress conditions of BC [19, 20]. According to the centrifuge model tests, Lee et al. [21] study the seismic performance of road box culverts and summarize seismic evaluation method of road box culverts. However, the research on the flexural capacity of BC is relatively limited, which is also a significant point to reflect the working efficiency of BC. Thus, the study of load bearing capacity of BC is also a great highlight.

Several studies have been conducted on reinforcement ratios of reinforced concrete (RC) structures. The bending performance of RC members increased with the increasing reinforcement ratio. The influence of reinforcement ratios on the bending performance and nonlinear fracture characteristics of alkali activated fly ash (AAFA) based on geopolymer concrete beams are conducted by using experiments and FEA [22]. And results showed that the increase of reinforcement ratios improves the ultimate bearing capacity of AAFA and reduces the cracks. Four lightweight aggregate concrete beams with reinforcement ratios of 1.12% and 2.96% are evaluated for the bending performance [23]. Feng et al. [24] conduct an investigation on the flexural behavior and cracking patterns of ultrahigh-performance concrete (UHPC) beams with different reinforcement ratios (0, 1.0%, 2.9%, 4.8%, and 7.1%) by four-point bending. And their results showed that increasing reinforcement ratios effectively decreases the development of deflection and has a positive effect on the load bearing capacity of the component. The social chaos caused by the earthquake can not be ignored, the seismic performance of RC structures with different reinforcement ratios is also hot topic [25, 26]. Noor-E-Khuda et al. [27] evaluate the effect of reinforcement ratios on the seismic performance of fully grouted reinforced masonry through FEA. Isufi et al. [28] analyze the seismic performance of slab–column connections with different bending reinforcement ratios from 0.64% to 1.34%. And these results showed that increasing reinforcement ratio is the vital factor to enhance seismic performance. However, investigation on the effect in different reinforcement forms with same reinforcement ratios on structural performance is relatively rarity. The reinforcement forms play a crucial role in increasing the loading capacity of BC.

Compared with the traditional concrete members, the prefabrication of building components off-site and their subsequent assembly on-site have numerous advantages of industrial processes, easy transportation, high degree of freedom, easy installation, convenient storage, and reduced consumption, which has been widely applied in the construction industry (steel structure, prefabricated frames, beam–column joints, shear walls, etc.) [29–32]. Presently, investigations on the behaviors of prefabricated structures under the shear load, flexural load, and cyclic load have been conducted [33–36]. Ding et al. [37] study the seismic performance of a semi-rigid connector between autoclaved lightweight concrete (ALC) panel and steel frame, which showed that the use of the semi-rigid connector can effectively reduce the damage of ALC panel. Pan et al. [38] study the seismic performance of prefabricated reinforced column–steel beams, and the results showed that specimens meet the seismic code requirements of strong columns and weak beams. The seismic performance of prefabricated frame–shear wall structures under cyclic loading is investigated [39]. The connection between prefabricated buildings is mainly based on dry connection, which has the advantages of high industrialization and construction efficiency. Shi et al. [40] analyze the bending behavior of UHPC precast composite beams with full-depth precast concrete slabs and propose a model to predict the flexural capacity and bending stiffness of UHPC composite beams. Although investigations on the performance of PS have been studied, research on the performance of PS of other form is needed. Therefore, further research on the performance of prefabricated box culvert (PBC) should be concerned.

The PBC was designed to eliminate the secondary pouring, welding, and bolting of components in the traditional prefabricated structure, simplifying the construction process, and improved construction efficiency. In order to study the performance of PBC in different reinforcement forms with same reinforcement ratios, the remainder of the paper was organized as follows: first of all, details of the dimensions, rebars, and concrete of the PBC were presented. Then, four-point bending tests were conducted to study the load bearing capacity of PBC. Furthermore, the model of PBC was established by FEA to compare the accuracy between experimental and simulated results. Moreover, PBC in different reinforcement forms with same reinforcement ratios according to the building code was studied to optimize the bending performance. Finally, some concluding remarks were presented.

2. Test and Analysis of the Load Bearing Capacity of the Box Culvert

2.1. Description of Specimens. The PBC was designed and conducted the section with dimensions of 2,600 mm in length, 1,000 mm in width, and 2,650 mm in height. The inner diameters of the section were 2,000 mm in length, 1,000 mm in width, and 2,000 mm in height, respectively, as shown in Figure 1. As shown in Figure 2, the PBC of tested specimens was composed of seven HRB400 rebars of 16 mm diameter with spacing 150 mm for longitudinal rebars, and HRB400 rebars of 14 mm diameter with spacing 200 mm for transverse rebars.

2.2. Material Properties. Three 16-mm rebars located at the longitudinal rebars of PBC and 14-mm rebars located at the transverse rebars of PBC were selected and tested for the mechanical properties, respectively. These properties are according to the Chinese Standard GB/T 228.1-2010 [41]. The material tests of rebars are shown in Figure 3 and the detail of mechanical indexes of rebars are shown in Table 1. The mixed proportions of concrete are listed in Table 2, and the water-to-binder ratio of concrete in PBC was 0.38. As shown in Figures 4 and 5, three blocks for concrete cube compressive and uniaxial compressive strengths are poured in the same

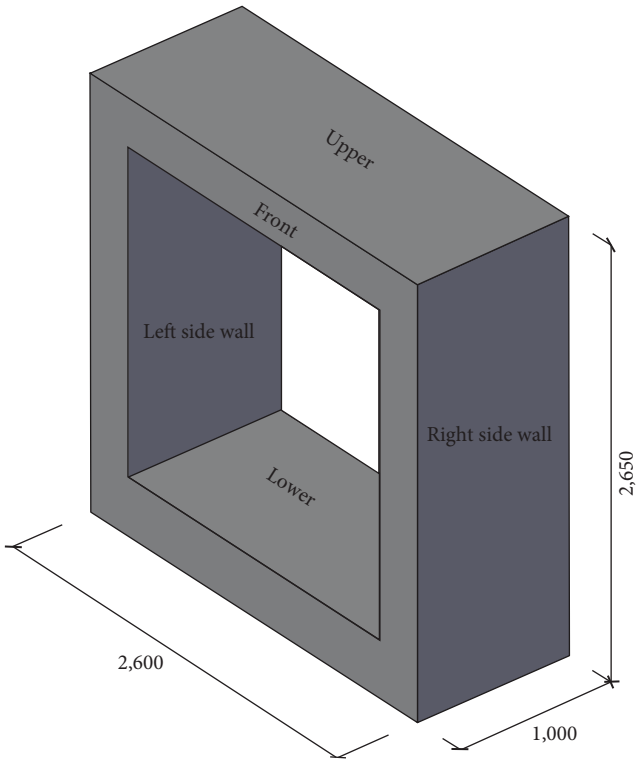

Figure 1: Three-dimensional diagram of PBC (dimension in mm).

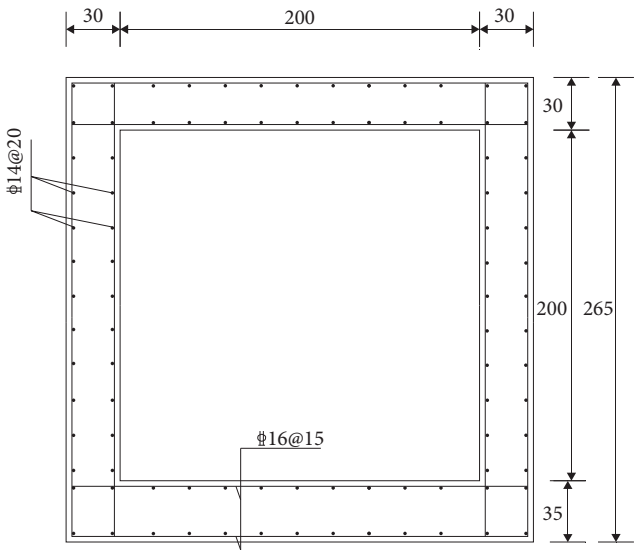

Figure 2: Rebars of the PBC (dimension in cm).

batch as the PBC and tested, respectively, which are according to Chinese Standard GB/T 50010-2010 [42]. The test results of cubic compressive strength f_{cu}, uniaxial compressive strength f_c, and elastic modulus E_c of concrete are listed in Table 3.

2.3. Instrumentation Layout and Test Setup. In order to fully explore the properties of PBC, the applied load, deformation, deflection, and strain of PBC were measured. As shown in Figure 6(a), 11 strain gauges were arranged in the upper of

Figure 3: Mechanical property test of rebars.

PBC to measure the strain of concrete. Among them, three were arranged at the 1/4 span, five were arranged at the midspan, and three were arranged at the 3/4 span. Eight flower-shaped strain gauges were arranged in the side wall of the PBC to measure strain of concrete. As shown in Figure 6(b), 38 gauges were embedded in the PBC to measure stress of rebars, among which two strain gauges were arranged in each marked position. The data were collected through the computerized data acquisition system, which analyzed the deflection and deformation of PBC during the experiment.

Static loading test was conducted in four-point bending, as shown in Figure 7. The loading devices were composed of loading cell, 2,000 kN jack, spreader beam, subordinate spreader beam, and hinged support. The loading cell was arranged above the 2,000 kN jack and connected with the reacting frame. The spreader beam was placed under the 2,000 kN jack, and the subordinate spreader beam was set under the main spreader beam. Two transversely placed hinged support under the subordinate spreader beam transferred the applied load to PBC. Besides, PBC was placed directly on the floor of the laboratory in accordance with actual working conditions. Three displacement sensors were arranged in the 1/4 span, midspan, and 3/4 span to measure the deflection of PBC. Eight displacement sensors were arranged in the corner and middle of the side wall to measure deformation and slip of the PBC. The data of loading cell and the displacement sensors were also collected by the data acquisition system, and the arrangement of strain measuring points and displacement measuring points is shown in Figure 8.

The loading history referred to GB/T 50152-2012 [43]. Before the load was the P_{ck} (P_{ck} was the cracking load), the 0.1 P_y (P_y was the yielding load) was taken as per stage (100 kN per stage). The second phase was taken 0.05 P_y per step (50 kN per stage) until PBC cracked. The third phase was taken 0.1 P_y per step (100 kN per stage) until PBC yielded. The final phase, 1 mm per stage was applied until PBC failure.

2.4. Test Results and Discussion. The failure mode of specimen PBC is depicted in Figure 9. During the early stage of

Table 1: Mechanical index of rebars.

	Diameter (mm)	Yielding strength (MPa)	Ultimate strength (MPa)	Elastic modulus (GPa)
	14	437.3	654.2	198.2
	14	448.9	656.7	195.3
	14	440.5	640.9	204.6
	16	447.8	658.8	207.2
	16	438.1	621.9	192.3
	16	433.4	661.5	205.1
Average value		441.0	649.0	200.5

Table 2: Mixed proportions of concrete (kg/m^3).

Cement	Fine	Sand	Coarse	Superplasticizer
251	135	835	1,120	6.46

Figure 4: Test of concrete cubic compressive strength.

Figure 5: Test of concrete uniaxial compressive strength.

loading phase, no obvious testing phenomenon occurred, and the PBC was in the elastic stage. When the load was 348.4 kN, the cracking noise of concrete was heard, and a crack firstly initiated at the pure bending section of the PBC. That indicated that the specimen entered the cracking stage. A number of cracks on the upper slab of PBC continuously increased with the increasing of vertical loads, and the left and right corners also gradually cracked with the increasing of vertical loads, as shown in Figure 9(a)–9(c). The maximum width of crack at the bottom of the right distribution beam was 0.5 mm under 721.5 kN. When the load was 1,055.6 kN, the crack at the bottom of the upper slab extended to the front. When the load was 1,246.9 kN, the left corner of the concrete suddenly fractured, as shown in Figure 9(d).

The curve of load–displacement has been proven to be an essential method for evaluating the load bearing capacity of PBC in the four-point bending, as reported in [44–46]. The load–displacement curve of PBC is shown in Figure 10. The curve can be mainly divided into three stages. In the first stage, no cracks were observed in PBC before the load was 348.4 kN. In the second stage, the curve was between the first inflection point and the second inflection point, and the loads were 348.4 and 1,055.6 kN, respectively. The load–displacement curve was slightly nonlinear, and cracks appeared on the concrete in the tensile zone of the PBC. In the third stage, PBC yielded under 1,055.6 kN, which shown a nonlinear state. Until the load was 1,246.9 kN, shear failure suddenly appeared in the bending–shear zone of upper slab of PBC, and the load bearing capacity of PBC suddenly decreased.

3. Numerical Simulation of the PBC

The FEA package ABAQUS was employed to build three-dimensional finite element model to verify the feasibility between experimental and simulated results.

3.1. Element Selection and Meshing. The 8-node linear brick with reduced integration and hourglass control element (C3D8R) was used for the distribution beams and concrete. Using T3D2 element for rebars was simplified methods for modeling convenience under the condition that they were mainly tensioned or compressed.

In order to generate mesh at parts level, all parts were selected as dependent parts and meshed by global seeds, which were function in the seed part of the mesh module controlling the seed size at a part level. The approximate global sizes of the concrete, spreader beam, and rebars were 50, 50, and 100 mm, respectively, modified by curvature

Table 3: Mechanical index of concrete.

	Cubic compressive strength (MPa)	Uniaxial compressive strength (MPa)	Elastic modulus (GPa)
	35.8	23.7	31.6
	33.4	22.4	30.9
	34.6	23.5	31.2
Average value	34.6	23.2	31.2

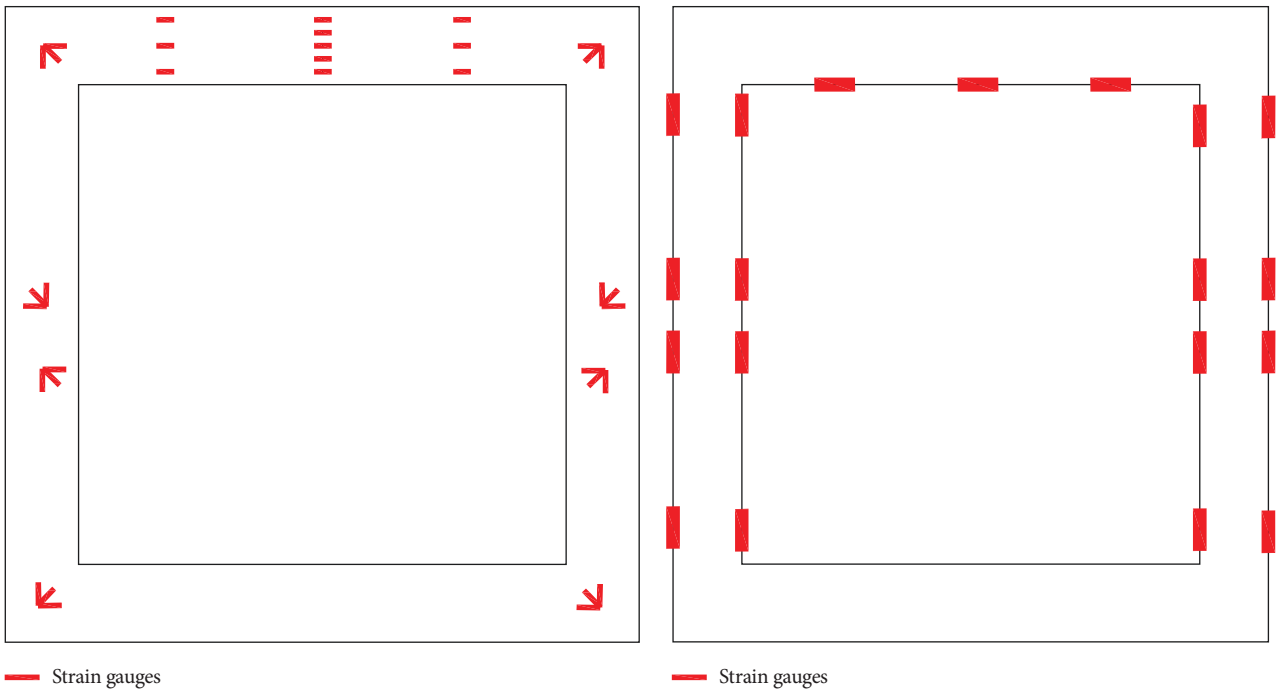

Figure 6: Sensor layout diagram. (a) Layout of strain gauges on surface of concrete and (b) layout of strain gauges on rebars.

control and minimum size control. Figure 11 shows the mesh of the whole model.

3.2. Material Properties of Model. As a model simulated concrete cracking, concrete damage plasticity (CDP) has been applied to the FEA of BC [17]. The tensile cracking and compressive crushing of concrete under low-confining pressures and monotonic, cyclic, and dynamic stresses can be reproduced by CDP. The study of key parameters of CDP has been shown in [47], which is helpful to improve the accuracy of the model. The material plastic parameters and the constitutive curve, in which the ratio biaxial to uniaxial compressive strength f_c was 1.16, dilation angle ψ was 30°, second stress invariant ratio K_c was 0.67, eccentricity ε was 0.1, and viscosity parameter μ was 0.001. According to the average of material test of concrete, the cubic compressive strength f_{cu} was 34.6 MPa, tensile strength f_t was 2.2 MPa, elastic modulus E_c was 31.2 GPa, and the Poisson ratio μ was 0.2, respectively.

Based on the Chinese Standard GB50010-2010 [42], the uniaxial compressive stress–strain relationship is calculated as follows:

$$\sigma = (1 - d_c) \cdot E_c \cdot \varepsilon, \tag{1}$$

$$d_c = \begin{cases} 1 - \dfrac{\rho_c \cdot n}{n - 1 + x^n}, & x \le 1 \\ 1 - \dfrac{\rho_c}{\alpha_c (x-1)^2 + x}, & x > 1 \end{cases}, \tag{2}$$

$$\rho_c = \frac{f_{c,r}}{E_c \varepsilon_{c,r} - f_{c,r}}, \tag{3}$$

$$n = \frac{E_c \varepsilon_{c,r}}{E_c \varepsilon_{c,r} - f_{c,r}}, \tag{4}$$

$$x = \frac{\varepsilon}{\varepsilon_{c,r}}, \tag{5}$$

where d_c denotes the uniaxial compression damage parameter; $f_{c,r}$ denotes the value of uniaxial compressive strength of concrete and takes as 23.2 MPa; α_c denotes the parameter of the constitutive curve descending section and takes as 0.74; and the peak compressive strain $\varepsilon_{c,r}$ is 0.00147, respectively.

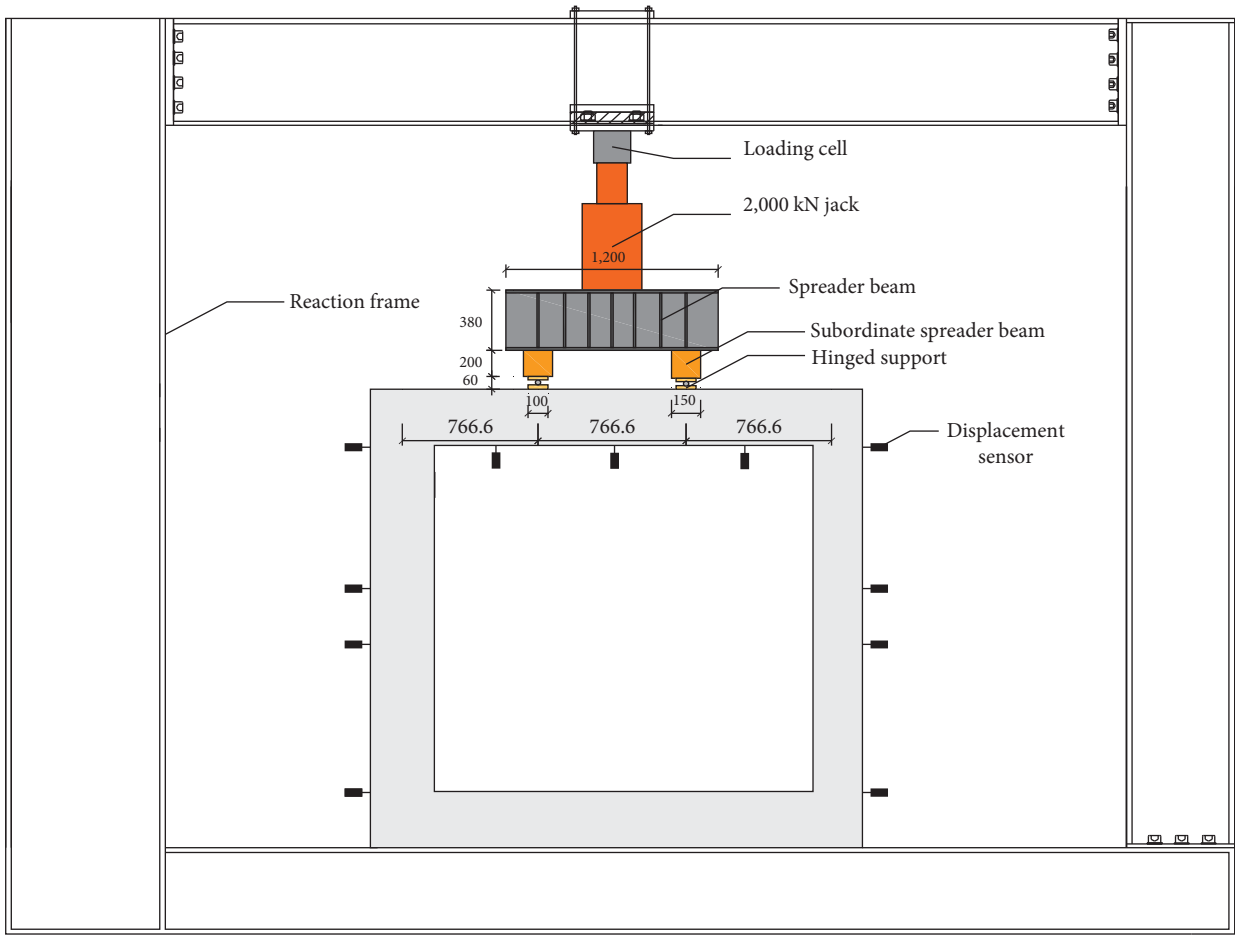

Figure 7: Diagram of test devices (dimension in mm).

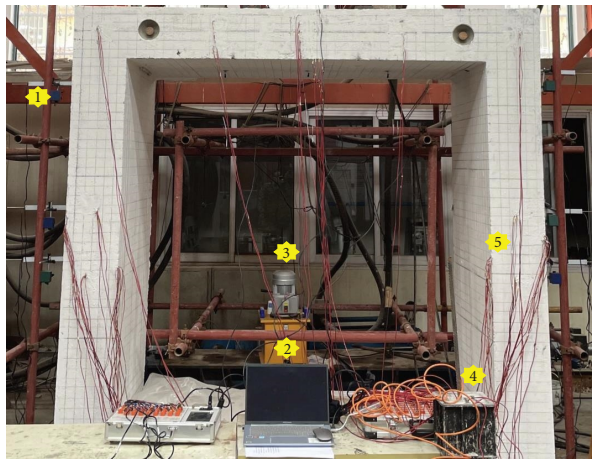

(1) Displacement sensor
(2) Dynamic signal acquisition and analysis system
(3) Motor driven oil pump
(4) Strain compensation specimen
(5) Strain gauges

Figure 8: Data acquisition system.

For tensile constitutive curve, the ascending section is considered as ideal elastic. The softening section based on fracture–energy theory is calculated as follows:

$$\frac{s(w)}{f_t} = \left[1 + \left(c_1 \cdot \frac{w}{w_c}\right)^3\right] \cdot \exp\left(-c_2 \cdot \frac{w}{w_c}\right) - \frac{w}{w_c} \cdot (1 + c_1^3) \cdot \exp(-c_2), \tag{6}$$

$$w_c = \frac{5.14 G_f}{f_t}, \tag{7}$$

where w denotes the crack opening; w_c denotes the critical opening; and fracture energy G_f, c_1, and c_2 are 100 J/m^2, 3, and 1.63, respectively.

The bilinear constitutive relationship is adopted to model the nonlinear behavior of rebars up to failure [48]. As shown in Figure 12, the average of mechanical testing result of HRB400 was used to calculate the bilinear constitutive curve, and the elastic modulus E_s, Poisson's ratio μ, yielding stress σ_y, ultimate tensile strength σ_u, strength hardening strain ε_{sh}, and ultimate

Figure 9: Cracking pattern of the PBC. (a) The bottom of upper slab, (b) the front, (c) the sidewall, and (d) the left corner.

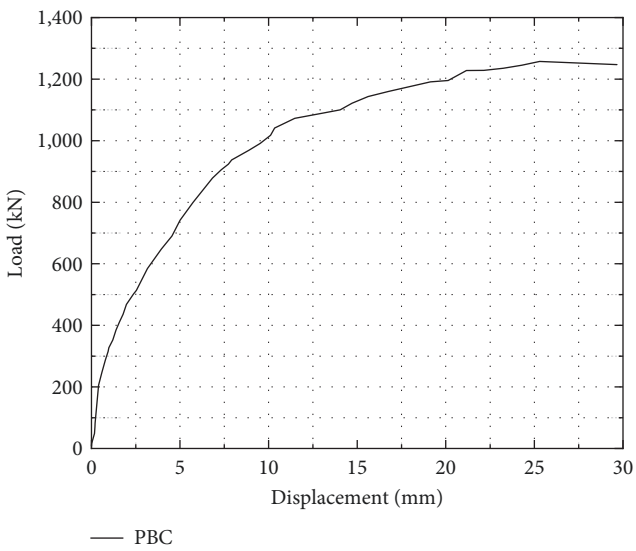

Figure 10: Load–displacement curve of PBC.

strength strain ε_u of HRB400 were 200.5 GPa, 0.3, 441 MPa, 649 MPa, 0.00221, and 0.1339, respectively. More material properties of rebars and concrete are shown in Table 4.

3.3. Create Analysis Steps. The static, general step was used to analyze the PBC model. One was the initial step which the boundary condition and gravity was applied. Another was step-1 which the load and gravity were adopted. The other was the restart request which was triggered to read data and continue the displacement phase analysis. The time period was mentioned in Section 2.3.

3.4. Interaction Condition of Model. Interaction definition between different model parts was particularly fundamental for accuracy of result and convergence of solution. This essential stage in a finite element problem reproduced the force transmission of the structure in reality. Three constraint types were employed in this study: tie, coupling, and embedded region. Figure 13 presents the diagram of model interaction, the tie was employed to spreader beam with the upper surface of the PBC and the lower surfaces of the beams were chosen to be the master surfaces, while the upper surface of the segment top slab was the slave surface. In the assembly, a reference point was created for controlling over the transmission of forces, and coupling constraint was employed to couple the motion of collection of nodes to the reference node, which simulated the process of a jack applying a load to a member. The reference point was coupled to

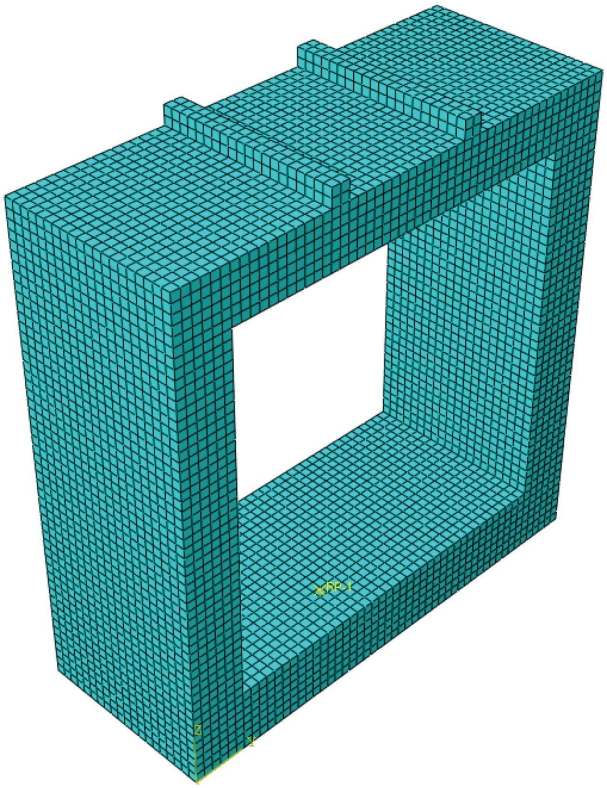

Figure 11: Mesh of the whole mode.

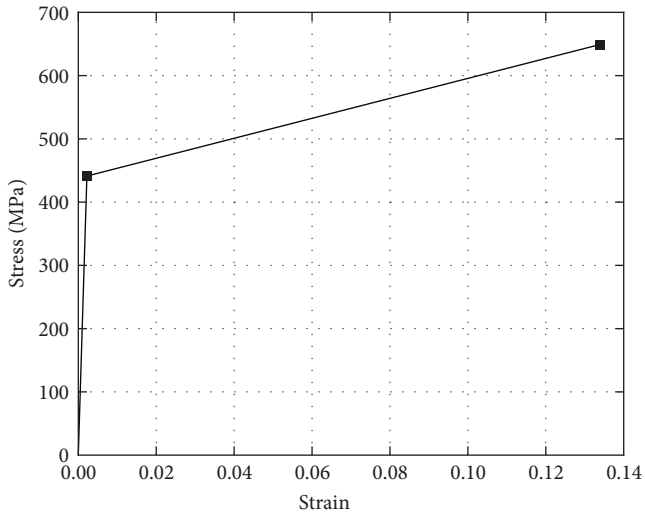

Figure 12: Constructive curve of rebars.

the top upper surfaces of the spreader beams with freedom of y direction constrained. The command of "embedded region" was employed to simulate the interaction between all the rebars and the concrete segment. The concrete segment is defined as the "host element" whereas the rebars are defined as the "embedded" elements [49].

3.5. Load and Boundary Conditions. The experimental process was reproduced in reality by applying concentrated forces or displacements to the coupling point. The bottom

Table 4: Material properties.

Material type	Density (kg/m^3)	Elastic modulus (MPa)	Poisson's ratio
HRB400	7,850	200,500	0.3
Concrete	2,400	31,200	0.2

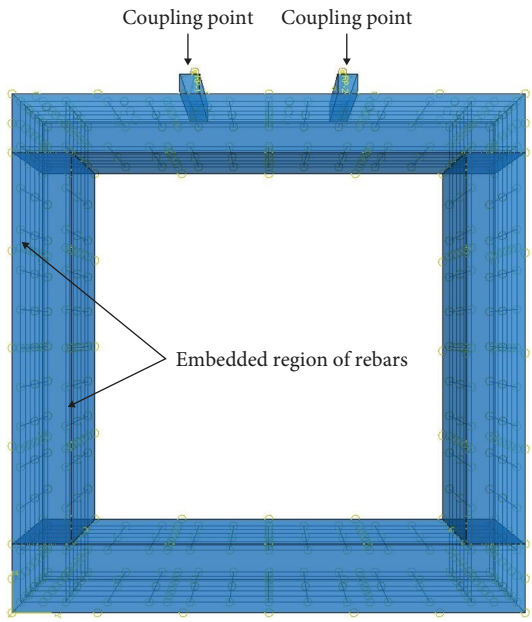

Figure 13: Diagram of model interaction.

surface of the segment X, Y, and Z directions were constrained by the translation and rotation ($UX = UY = UZ = URX = URY = URZ = 0$), which accurately reproduced the situation where PBC was placed directly on the laboratory floor, as shown in Figure 14.

3.6. Verification of Finite Element Results. The member is considered to fail when the concrete strain at the top of the compression zone is 0.003 as well as the stress of rebars exceed the yielding strength, as reported in [50–52]. Figure 15 depicts the comparison of simulated and experimental results. From the results of the load–displacement curve, the initial slope of the simulated curve was greater than the experimental results. The tendency of experimental and simulated curve was the approximate identity. Besides, the ultimate loads of the experimental and simulated results were 1,246.9, and 1,311.6 kN, respectively. The maximum deviation of ultimate load of PBC between simulated and experimental results was only 5.19%. The horizontal branch beyond yield in the simulated results was longer than that in the experimental test, because the slip of concrete and rebars was not considered. However, all differences were within acceptable ranges, and the simulated results of PBC were consistent with the experimental results.

The compared results of plastic damage distribution of concrete (DAMAGET) and experiment for PBC were shown in Figure 16. The DAMAGET area of concrete was observed

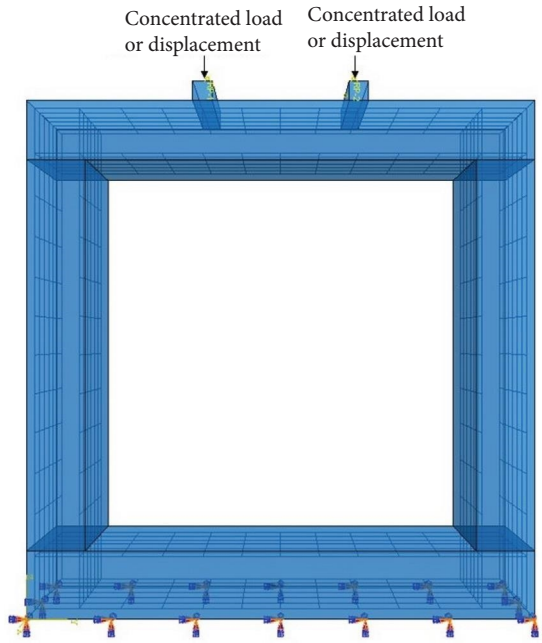

Figure 14: Diagram of load setting and displacement constraint of PBC.

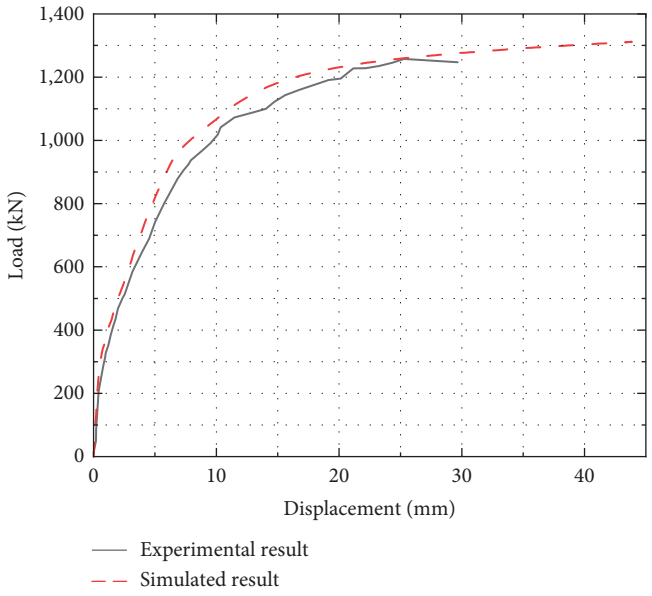

Figure 15: Comparison of simulated and experimental results.

in the upper slab and the outside of the side wall, which were the same as the experimental results. Note that the higher value and area of DAMAGET of PBC have, the more severe plastic damage in concrete of PBC get [53]. The high value of DAMAGET of simulated results was observed in the simulation, which was consistent with a large area of damage on the corner and upper slab of PBC in the experiment. The results of DAMAGET further proved the accuracy of the finite-element model.

4. Effect of Reinforcement Forms on the Load Bearing Capacity

Many scholars have studied the influence of different reinforcement ratios on the mechanical properties of the concrete members, and the results show that the increasing reinforcement ratios are substantial in enhancing the ultimate load bearing capacity of concrete members [22, 24, 54, 55]. However, the reinforcement forms also have crucial impact on the concrete members [56]. In order to study the influence of reinforcement forms on the performance of PBC, models in different reinforcement forms with same reinforcement ratios were analyzed according to load bearing capacity, stress of rebars, PEEQ, DMAGET, and ductility. Table 5 shows specimen details for the model tests of PBC in different reinforcement forms with same reinforcement ratios.

4.1. Analysis of Loading Displacement Curves. The relationship between different reinforcement forms and load–displacement curves of PBC shows same trends, as shown in Figure 17. When the PBC was the failure standard, loads or displacements of PBC-7T16, PBC-7T18, PBC-6T18, and PBC-5T20 were 1311.64, 1347.93, 1199.30, and 1,251.24 kN or 43.85, 63.11, 24.66, and 42.94 mm, respectively. The ultimate loads of PBC-7T18, PBC-6T18, and PBC-5T20 increased by 2.77%, −8.56%, and −4.65% compared with those of experimental model (PBC-7T16), respectively. The displacements of midspan of specimen PBC-7T18 were larger than that of specimen PBC-7T16. Beyond yielding load, the growth rate of deformation of specimen PBC-7T18 was evidently lower than that of reference specimen PBC-7T16, although the yielding displacement of PBC-7T18 was smaller than that of PBC-7T16. The specimen PBC-7T18 had a better performance in the mechanics compared with that of reference specimen PBC-7T16. Therefore, the load-bearing capacity of PBC increased by changing the reinforcement forms with same reinforcement ratios, in particularly the PBC-7T18 had higher load bearing capacity than that of PBC-7T16.

4.2. Analysis of Stress Cloud. Figure 18(a)–18(d) reveals the stress of rebars of specimens PBC-7T16, PBC-7T18, PBC-6T18, and PBC-5T20, respectively. The yielding rebars were mainly appeared in the midspan and upper corner, while the location of maximum stress was appeared in the midspan. However, the stress distribution of compressive rebars in the PBC upper slab and the rebars in the side wall was obviously different. Additionally, compared with PBC-7T16, notable reduction of stress occurred in the tensile area rebars around the upper slab and side wall of PBC-7T18, PBC-6T18, and PBC-5T20. The maximum stress of rebars of PBC-7T18, PBC-6T18, and PBC-5T20 were 482.0, 453.3, and 477.4 MPa, which were smaller than that of PBC-7T16 of 503.8 MPa. The compressive strain of PBC-6T18 and PBC-5T20 concrete got the failure standard earlier than that of PBC-7T16. Compared with the other specimens, the tensile rebars of PBC-7T18 had larger yielding area, avoided severely local yielding of the longitudinal rebars, and played a more active role in

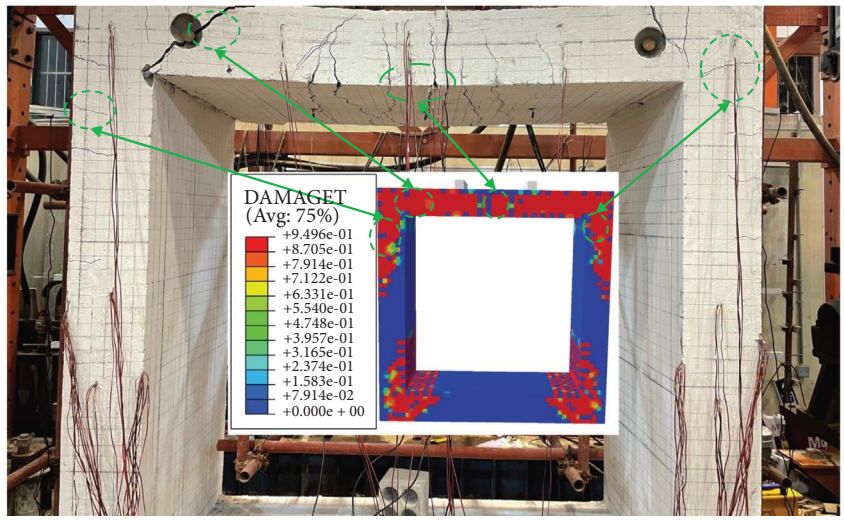

Figure 16: Compared results of simulated and experimental of DAMAGET.

Table 5: Specimen details for model tests of PBC.

Specimen	Rebars (mm)		Reinforcement ratio (ρ)
	Inner	Outer	
PBC-7T16	7φ16	7φ16	0.938%
PBC-7T18	7φ18	7φ14	0.953%
PBC-6T18	6φ18	6φ16	0.911%
PBC-5T20	5φ20	5φ18	0.947%

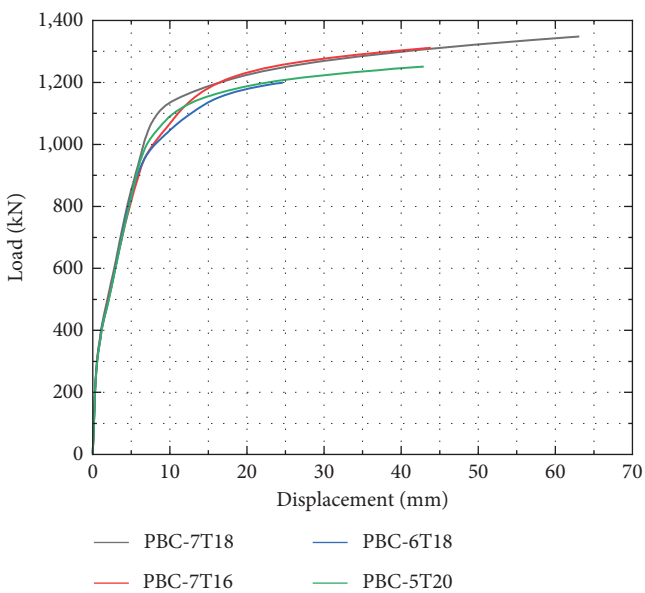

Figure 17: Load–displacement curves of variable parameter of PBC.

increasing its load bearing capacity. Similar conclusions of different reinforcement forms of specimens are also reported in [57].

4.3. Analysis of DAMAGET. According to Figure 19, the DAMAGET of PBC with different reinforcement forms was in the identical interval and value increased from 0.0791 to 0.9496 under the failure standard. The approximately identical area of concrete damage was observed in the PBC upper slab. More specifically, the concentrated area of concrete damage of PBC was observed in the upper slab and corner, while no significant damage appeared the middle of the side wall and bottom slab. Compared with PBC-7T16, the degree of damaged concrete significantly reduced around the top of the side wall and the bottom corner of PBC-7T18, PBC-6T18, and PBC-5T20. The results showed that the cracking of concrete was effectively reduced by increasing the area of tensile rebars of PBC with reducing the area of compressive rebars of PBC under same reinforcement ratios, which was beneficial for increasing the load bearing capacity of PBC. Similar tendency in the development of DAMAGET of concrete components can also be found in [58].

4.4. Analysis of PEEQ. Figure 20 depicts the comparison of simulated results of PEEQ. The similar distribution area of PEEQ was observed in models of different reinforcement forms with same reinforcement ratios. The PEEQ primarily concentrated around the upper slab and corners of PBC. In detail, the maximum damage points of PBC-7T16, PBC-6T18, and PBC-5T20 occurred around the compressive area of concrete of upper slab. However, the maximum damage point of PBC-7T18 occurred around the tensile area of concrete of upper slab. Furthermore, the plastic damage around the connection between the upper slab and the side wall of PBC-7T18–PBC-5T20 was more severe than that of PBC-7T16, which was caused by the different diameters of the inner and outer rebars. The stress concentration occurred at the connection between the inner and outer rebars was key factor, which triggered tendency toward shear failure in both the rebars and concrete at the interface of the side wall and upper slab. The smaller PEEQ area and value of PBC-7T18–PBC-5T20 were detected than that of PBC-7T16. By changing the reinforcement forms with same reinforcement ratios, the plastic deformation characteristics of PBC increased, which were advantageous for increasing its load

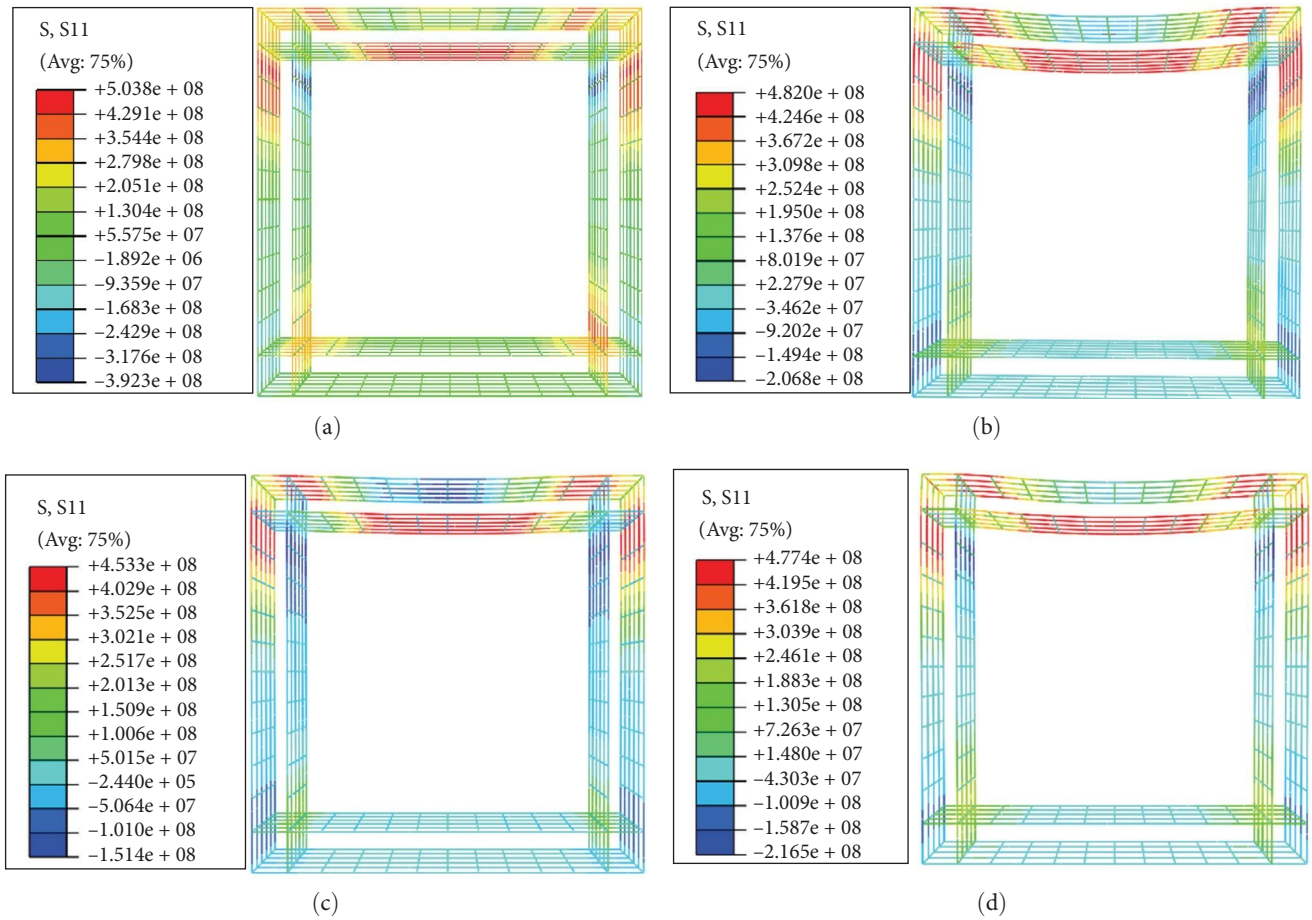

Figure 18: Simulated results of stress of rebars. (a) PBC-7T16, (b) PBC-7T18, (c) PBC-6T18, and (d) PBC-5T20.

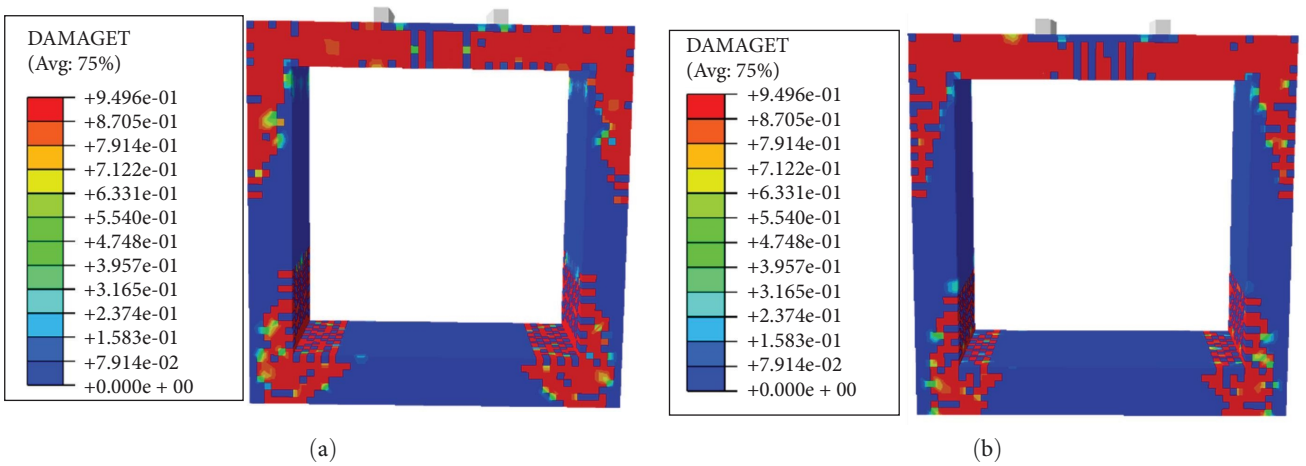

Figure 19: Continued.

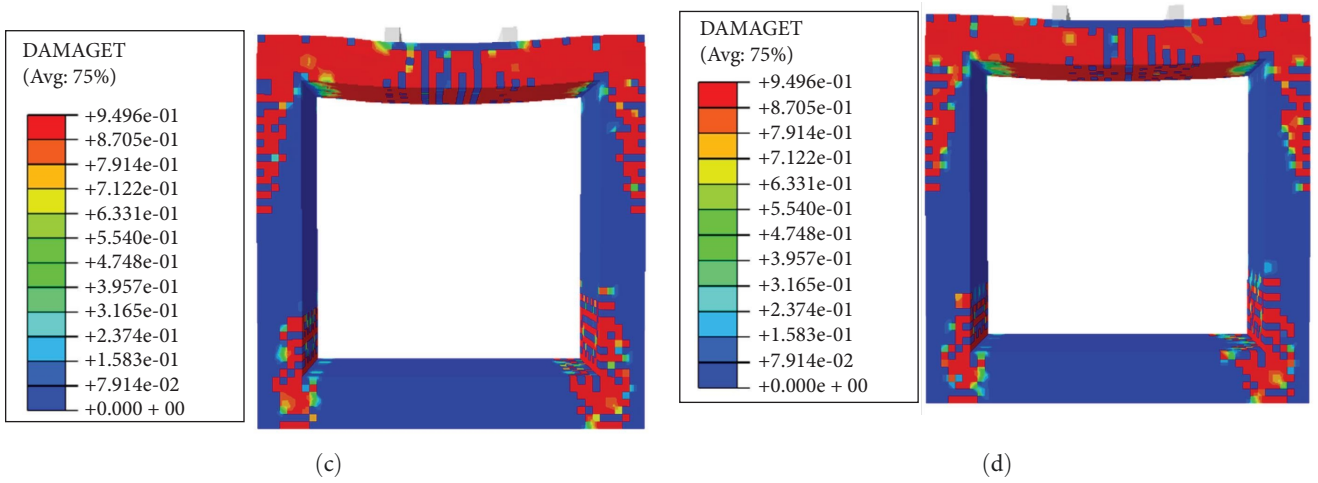

Figure 19: Simulated results of DAMAGET. (a) PBC-7T16, (b) PBC-7T18, (c) PBC-6T18, and (d) PBC-5T20.

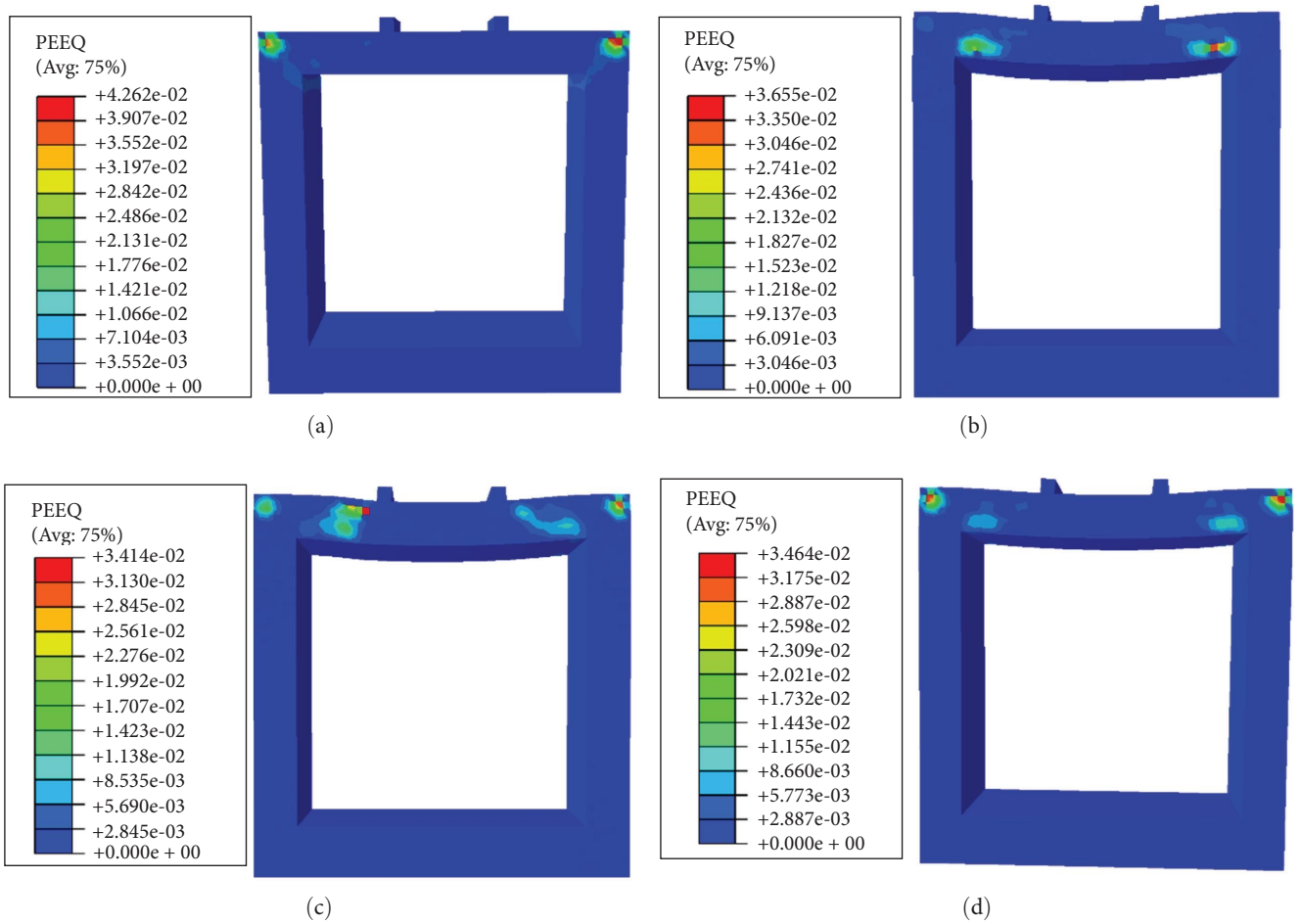

Figure 20: Comparison of simulated results of PEEQ. (a) PBC-7T16, (b) PBC-7T18, (c) PBC-6T18, and (d) PBC-5T20.

bearing capacity, especially evident in the case of the PBC-7T18 under the four-point bending.

4.5. Analysis of Ductility. Ductility is considered the ability of the member to resist deformation when the load passing the yielding point [59–61]. A great deal of energy was absorbed in the inelastic deformation process of concrete ductile members. Generally, the yielding displacement Δ_y, ultimate displacement Δ_u, and displacement ductility ratio μ were utilized to evaluate the ductility performance.

Table 6: Test results of all specimens.

Specimen	P_y (kN)	Δ_y (mm)	P_u (kN)	Δ_u (mm)	μ	Ratio of ductility of parameters specimens to PBC-7T16
PBC-7T16	1062.56	9.86	1311.64	43.85	4.45	100%
PBC-7T18	1114.52	8.95	1347.93	63.11	7.05	158.4%
PBC-6T18	988.64	7.69	1199.30	24.66	3.21	72.1%
PBC-5T20	1038.26	8.08	1251.24	42.94	5.31	119.3%

Note. P_y is the yielding load, P_u is the ultimate load, Δ_y is the yielding displacement, and Δ_u is the ultimate displacement.

$$\mu = \frac{\Delta_u}{\Delta_y}, \tag{8}$$

where Δ_u and Δ_y are displacement measured by the midspan displacement at the ultimate failure and yield of PBC.

The ductility indices were calculated by models of PBC in the present study, and the results are shown in Table 6. Contrasting with the reference specimen PBC-7T16, the yielding or ultimate load of specimens PBC-7T18, PBC-6T18, and PBC-5T20 increased by 4.89%, −6.95%, and −2.29% or 2.77%, −8.56%, and −4.60%, respectively. The yielding and ultimate loads of PBC models were improved by strengthening rebars. Additionally, the ductility of specimens PBC-7T18, PBC-6T18, and PBC-5T20 increased by 58.4%, −27.9%, and 19.3% contrasting with reference specimen PBC-7T16, respectively. The evident increase in ultimate displacement of specimen PBC-7T18 was found contrasted with that of reference specimen PBC-7T16. Except the result of PBC-6T18, the ductility significantly increased by changing reinforcement forms with same reinforcement ratios, which were beneficial for increasing the ability resist deformation PBC under the four-point bending.

5. Conclusion

In this paper, the PBC was designed and tested by four-point bending to analysis the load bearing capacity of PBC, and the effect in different reinforcement forms with same reinforcement ratios of PBC on load bearing capacity by FEA was also conducted. The main conclusions could be drawn as follows:

(1) The yielding load, ultimate load, yielding displacement, and ultimate displacement of tested PBC were 1,055.6, 1,246.9, 10.86, and 29.66 mm, respectively. A number of flexural cracks were observed in the midspan bottom of upper slab of PBC during the experiment. When the load was 1,246.9 kN, the final shear failure was observed in the bending–shear zone of PBC.

(2) The simulated and experimental results of PBC had a good agreement. The maximum deviation of ultimate load of PBC between the experimental and simulated results was only 5.19%. The DAMAGET of the PBC model had same damage area with the experimental results.

(3) The ultimate load of PBC-7T18 was 2.7% higher than that of specimen PBC-7T16. Increasing the area of tensile rebars with reducing the area of compressive rebars played active role in enhancing the load bearing capacity of PBC in different reinforcement forms with same reinforcement ratios, especially in using the 7φ18 mm tensile rebars of PBC.

(4) In same reinforcement ratios, the number of concrete cracking, plastic deformation, and stress on the rebars effectively decreased by increasing the area of tensile rebars with reducing the area of compressive rebars. The ductility of PBC in different reinforcement forms with same reinforcement ratios also increased contrasted with those of reference specimen. Altering reinforcement forms with same reinforcement ratios were beneficial for increasing the load bearing capacity of PBC.

Data Availability

Data supporting this research article are available on request from the authors.

Conflicts of Interest

The authors declare that they have no conflicts of interest.

Authors' Contributions

Yajun Xie and Pengfei Xu contributed in the formal analysis. Li Wang, Pengfei Xu, and Jian Chen contributed in the investigation. Li Wang, Jian Chen, and Ming Li contributed in the validation. Ming Li contributed in the conceptualization and methodology. Rui Guo contributed in the data curation. Da Zong contributed in the software, writing —original draft, and writing — review and editing.

Acknowledgments

The financial support of the Water Science and Technology Project of Jiangsu Province (Grant No. 2020019) is gratefully acknowledged.

References

[1] Y. Gong, Y. Ma, G. Tan, H. Bi, Y. Pang, and C. Ma, "Experimental study and numerical simulation on failure process of reinforced concrete box culvert," *Advances in Civil Engineering*, vol. 2020, Article ID 5423706, 13 pages, 2020.

[2] Y. Gong, S. Lin, F. He, Y. He, and J. Song, "Damage identification of prefabricated reinforced concrete box culvert

based on improved fuzzy clustering algorithm and acoustic emission parameters," *Advances in Materials Science and Engineering*, vol. 2021, Article ID 6660915, 13 pages, 2021.

[3] M. Pimentel, P. Costa, C. Félix, and J. Figueiras, "Behavior of reinforced concrete box culverts under high embankments," *Journal of Structural Engineering*, vol. 135, no. 4, pp. 366–375, 2009.

[4] A. K. Garg, A. Abolmaali, and R. Fernandez, "Experimental investigation of shear capacity of precast reinforced concrete box culverts," *Journal of Bridge Engineering*, vol. 12, no. 4, pp. 511–517, 2007.

[5] S.-Q. Wang, D.-C. Feng, and G. Wu, "Design and bearing capacity test of prefabricated high-strength thin concrete segments for reinforcing underground box culverts," *Engineering Failure Analysis*, vol. 142, Article ID 106844, 2022.

[6] S. L. Orton, J. E. Loehr, A. Boeckmann, and G. Havens, "Live-load effect in reinforced concrete box culverts under soil fill," *Journal of Bridge Engineering*, vol. 20, no. 11, Article ID 04015003, 2015.

[7] T. A. Wood, W. D. Lawson, P. W. Jayawickrama, and C. D. Newhouse, "Evaluation of production models for load rating reinforced concrete box culverts," *Journal of Bridge Engineering*, vol. 20, no. 1, Article ID 04014057, 2015.

[8] B. G. Chen, J. J. Zheng, and J. Han, "Experimental study and numerical simulation on concrete box culverts in trenches," *Journal of Performance of Constructed Facilities*, vol. 24, no. 3, pp. 223–234, 2010.

[9] G. Zenagebriel, J. Li, and G. Qiao, "Experimental and finite element analysis of precast reinforced concrete U-shaped box culvert," *Iranian Journal of Science and Technology, Transactions of Civil Engineering*, vol. 45, pp. 2133–2143, 2021.

[10] B. Chen, D. Song, X. Mao, E. J. Chen, and J. Zhang, "Model test and numerical simulation on rigid load shedding culvert backfilled with sand," *Computers and Geotechnics*, vol. 79, pp. 31–40, 2016.

[11] P. Li, S. Liu, J. Ji, X. Ding, and M. Bao, "Stochastic analysis of excavation-induced wall deflection and box culvert settlement considering spatial variability of soil stiffness," *Journal of Rock Mechanics and Geotechnical Engineering*, 2023.

[12] J. N. Varandas, P. Hölscher, and M. A. G. Silva, "Three-dimensional track-ballast interaction model for the study of a culvert transition," *Soil Dynamics and Earthquake Engineering*, vol. 89, pp. 116–127, 2016.

[13] S. H. Kim, S. H. A. Shah, S. K. Woo, I. Chu, and C. Sim, "Probability-based crack width estimation model for flexural members of underground RC box culverts," *Applied Sciences*, vol. 12, no. 4, Article ID 2063, 2022.

[14] M. Moradi, H. Valipour, and S. Foster, "Reserve of strength in inverted U-shaped RC culverts: effect of backfill on ultimate load capacity and fatigue life," *Journal of Bridge Engineering*, vol. 21, no. 2, Article ID 04015051, 2016.

[15] A. K. Garg and A. Abolmaali, "Finite-element modeling and analysis of reinforced concrete box culverts," *Journal of Transportation Engineering*, vol. 135, no. 3, pp. 121–128, 2009.

[16] G. Yang, G. Wang, W. Lu, X. Zhao, P. Yan, and M. Chen, "Numerical modeling of surface explosion effects on shallow-buried box culvert behavior during the water diversion," *Thin-Walled Structures*, vol. 133, pp. 153–168, 2018.

[17] H. A. Waqas, M. Waseem, A. Riaz, M. Ilyas, M. Naveed, and H. Seitz, "Influence of Haunch geometry and additional steel reinforcement on load bearing capacity of reinforced concrete box culvert," *Materials*, vol. 16, no. 4, Article ID 1409, 2023.

[18] S. Philip, R. Rakendu, and R. Lal, "The impact of geofoam on the bending moment characteristics of reinforced concrete box culverts for road under bridge (RUB) design," *Materials Today: Proceedings*, vol. 52, pp. 2305–2314, 2022.

[19] G. Zhang, Y. Hu, and J.-M. Zhang, "New image analysis-based displacement-measurement system for geotechnical centrifuge modeling tests," *Measurement*, vol. 42, no. 1, pp. 87–96, 2009.

[20] B. L. Kutter, "Dynamic centrifuge modeling of geotechnical structures," *Transportation Research Record*, no. 1336, pp. 24–30, 1992.

[21] K. Lee, J. Kim, and S. I. Woo, "Analysis of horizontal earth pressure acting on box culverts through centrifuge model test," *Applied Sciences*, vol. 12, no. 4, Article ID 1993, 2022.

[22] K. Zerfu and J. J. Ekaputri, "The effect of reinforcement ratio on the flexural performance of alkali-activated fly ash-based geopolymer concrete beam," *Heliyon*, vol. 8, no. 12, Article ID e12015, 2022.

[23] D. Dias-da-Costa, R. N. F. Carmo, R. Graça-e-Costa, J. Valença, and J. Alfaiate, "Longitudinal reinforcement ratio in lightweight aggregate concrete beams," *Engineering Structures*, vol. 81, pp. 219–229, 2014.

[24] Z. Feng, C. Li, D. Y. Yoo, R. Pan, J. He, and L. Ke, "Flexural and cracking behaviors of reinforced UHPC beams with various reinforcement ratios and fiber contents," *Engineering Structures*, vol. 248, Article ID 113266, 2021.

[25] X. Y. Cao, D. C. Feng, and Y. Li, "Assessment of various seismic fragility analysis approaches for structures excited by non-stationary stochastic ground motions," *Mechanical Systems and Signal Processing*, vol. 186, Article ID 109838, 2023.

[26] X. Y. Cao, D. C. Feng, and M. Beer, "Consistent seismic hazard and fragility analysis considering combined capacity–demand uncertainties via probability density evolution method," *Structural Safety*, vol. 103, Article ID 102330, 2023.

[27] S. Noor-E-Khuda and D. P. Thambiratnam, "In-plane and out-of-plane structural performance of fully grouted reinforced masonry walls with varying reinforcement ratio—a numerical study," *Engineering Structures*, vol. 248, Article ID 113288, 2021.

[28] B. Isufi, M. Rossi, and A. P. Ramos, "Influence of flexural reinforcement on the seismic performance of flat slab–column connections," *Engineering Structures*, vol. 242, Article ID 112583, 2021.

[29] X. Y. Cao, D. C. Feng, C. L. Wang, D. Shen, and G. Wu, "A stochastic CSM-based displacement-oriented design strategy for the novel precast SRC-UHPC composite braced-frame in the externally attached seismic retrofitting," *Composite Structures*, vol. 321, Article ID 117308, 2023.

[30] L. Xie, Y. Chen, B. Xia, and C. Hua, "Importance-performance analysis of prefabricated building sustainability: a case study of Guangzhou," *Advances in Civil Engineering*, vol. 2020, Article ID 8839118, 17 pages, 2020.

[31] Y. H. Zhao, "Features and construction of prefabricated buildings," *Applied Mechanics and Materials*, vol. 580-583, pp. 2262–2265, 2014.

[32] R. He, Z. Zhang, and J. Li, "Experimental study on bolt-spliced prefabricated steel frame beams," *Advances in Civil Engineering*, vol. 2020, Article ID 6191475, 12 pages, 2020.

[33] M. Heweidak, B. Kafle, and R. Al-Ameri, "Shear-bond behaviour of profiled composite slab incorporated with self-compacted geopolymer concrete," *Applied Sciences*, vol. 12, no. 17, Article ID 8512, 2022.

[34] K. Jin, R. Ota, L. Hao, and K. Kitayama, "Evaluation method for ultimate fexural state of prestressed porecast reinforced concrete beam–column connection with debonded partial tendon," *Applied Sciences*, vol. 13, no. 5, Article ID 2843, 2023.

[35] K. Wang, K. Ding, and T. Yang, "Experimental study on the seismic performance of new energy dissipation connectors in an autoclaved aerated concrete panel with assembled steel frame," *Applied Sciences*, vol. 12, no. 24, Article ID 13035, 2022.

[36] Q. Liu, S. Chen, W. Lin, and F. Zeng, "Experimental study on novel energy-dissipating prefabricated beam–column joints," *Advances in Civil Engineering*, vol. 2019, Article ID 8151087, 17 pages, 2019.

[37] K. Ding, D. Zong, Y. Liu, S. He, and W. Shen, "Experimental and finite element analysis of external ALC panel steel frames with new semi-rigid connector," *Applied Sciences*, vol. 11, no. 22, Article ID 10990, 2021.

[38] Z. Pan, Q. Si, Y. Zhu, H. Ying, X. Wang, and D. Du, "Seismic performance of prefabricated semi-rigid RCS structures," *Structures*, vol. 43, pp. 1369–1379, 2022.

[39] L. Jia, Q. Li, Y. Zhang, W. Zhao, and M. Du, "Experimental study of the hysteretic behavior of prefabricated frame–shear wall structures with grouting sleeve connections," *Journal of Building Engineering*, vol. 57, Article ID 104704, 2022.

[40] F. W. Shi, C. H. Sun, X. G. Liu, H. Wang, and L. Zong, "Flexural behavior of prefabricated composite beam with cast-in-situ UHPC: experimental and numerical studies," *Structures*, vol. 45, pp. 670–684, 2022.

[41] Chinese Standard, "Metallic materials-tensile testing-part 1: method of test at room temperature GB/T 228.1-2010," National Steel Standardization Technical Committee (in Chinese), 2010.

[42] Chinese Standard, *Code for Design of Concrete Structures GB 50010-2010*, Ministry of Housing and Urban-Rural Development of the People's Republic of China, Beijing, China, (in Chinese), 2010.

[43] Chinese Standard, "Standard for test method of concrete structures GB/T 50152-2012, Ministry of Housing and Urban Rural Development of the People's Republic of China," (in Chinese), 2012.

[44] D. Shen, S. Deng, J. Zhang, W. Wang, and G. Jiang, "Behavior of reinforced concrete box beam with initial cracks repaired with basalt fiber-reinforced polymer sheet," *Journal of Reinforced Plastics and Composites*, vol. 34, no. 18, pp. 1540–1554, 2015.

[45] D. Shen, Y. Jiao, M. Li, C. Liu, and W. Wang, "Behavior of a 60-year-old reinforced concrete box beam strengthened with basalt fiber-reinforced polymers using steel plate anchorage," *Journal of Advanced Concrete Technology*, vol. 19, no. 11, pp. 1100–1119, 2021.

[46] D. Shen, X. Zeng, J. Zhang, B. Zhou, and and W. Wang, "Behavior of RC box beam strengthened with basalt FRP using end anchorage with grooving," *Journal of Composite Materials*, vol. 53, no. 23, pp. 3307–3324, 2019.

[47] Y. Xiao, Z. Chen, J. Zhou, Y. Leng, and R. Xia, "Concrete plastic-damage factor for finite element analysis: concept, simulation, and experiment," *Advances in Mechanical Engineering*, vol. 9, no. 9, 2017.

[48] L. Guo, S. Gao, F. Fu, and Y. Wang, "Experimental study and numerical analysis of progressive collapse resistance of composite frames," *Journal of Constructional Steel Research*, vol. 89, pp. 236–251, 2013.

[49] G. Kenea and A. Feyissa, "Cyclic behavior of reinforced concrete slab–column connection using numerical simulation," *Advances in Civil Engineering*, vol. 2022, Article ID 2814715, 14 pages, 2022.

[50] R. A. Hawileh, H. A. Musto, J. A. Abdalla, and M. Z. Naser, "Finite element modeling of reinforced concrete beams externally strengthened in flexure with side-bonded FRP laminates," *Composites Part B: Engineering*, vol. 173, Article ID 106952, 2019.

[51] R. Hawileh, M. Z. Naser, and J. A. Abdalla, "Finite element simulation of reinforced concrete beams externally strengthened with short-length CFRP plates," *Composites Part B: Engineering*, vol. 45, no. 1, pp. 1722–1730, 2013.

[52] T. Yang and R. Xie, "Flexural behaviors of prefabricated composite beams with segmented precast concrete slabs," *Journal of Constructional Steel Research*, vol. 201, Article ID 107692, 2023.

[53] Hibbitt, Karlsson and Sorensen, "ABAQUS/standard: User's Manual," vol. 1, 1997.

[54] Y. Du, J. Wang, C. Shi, H. J. Hwang, and N. Li, "Flexural behavior of alkali-activated slag-based concrete beams," *Engineering Structures*, vol. 229, Article ID 111644, 2021.

[55] C. Wu, H. J. Hwang, C. Shi, N. Li, and Y. Du, "Shear tests on reinforced slag-based geopolymer concrete beams with transverse reinforcement," *Engineering Structures*, vol. 219, Article ID 110966, 2020.

[56] M. S. Aydogan, C. Aydemir, and G. Arslan, "An experimental and analytical research on moment redistribution in reinforced concrete continuous beams," *European Journal of Environmental and Civil Engineering*, pp. 1–24, 2023.

[57] B. Lu, C. Gno, and W. Gong, "Experiment on the forms of reinforcement affecting load bearing behavior of deep pile caps," *Industrial Construction*, vol. 38, no. 4, pp. 54–58, 2008.

[58] X. Han and Z. Liu, "Numerical simulation on the form of reinforcement of reinforced concrete beam with openings," *Applied Mechanics and Materials*, vol. 444-445, pp. 884–888, 2013.

[59] M. Li, D. Shen, Q. Yang, X. Cao, C. Liu, and J. Kang, "Rehabilitation of seismic-damaged reinforced concrete beam–column joints with different corrosion rates using basalt fiber-reinforced polymer sheets," *Composite Structures*, vol. 289, Article ID 115397, 2022.

[60] D. Shen, M. Li, J. Kang, C. Liu, and C. Li, "Experimental studies on the seismic behavior of reinforced concrete beam–column joints strengthened with basalt fiber-reinforced polymer sheets," *Construction and Building Materials*, vol. 287, Article ID 122901, 2021.

[61] D. Shen, M. Li, C. Liu, J. Kang, C. Li, and J. Yang, "Seismic performance of corroded reinforced concrete beam–column joints repaired with BFRP sheets," *Construction and Building Materials*, vol. 307, Article ID 124731, 2021.